Annual Report for NASA Grant NAGW - 3150

The Analysis of Global Cloud and Radiation Data for the Study of Cloud-Climate Interactions

P.I.: Harshvardhan
Department of Earth and Atmospheric Sciences
Purdue University
West Lafayette, Indiana 47907-1397

January 1, 1993 - December 31, 1993

The Analysis of Global Cloud and Radiation Data for the Study of Cloud-Climate Interactions

NASA Grant NAGW - 3150

During the past year, graduate student Kathryn Ginger has analyzed ISCCP C1 data for two regions, the stratocumulus area off California and the tropical Atlantic. Her work has led to an M.S. thesis which is in the process of being submitted in its final form. Copies will be mailed to the Technical Officer and the NASA Center for Aerospace Information when it is ready for dissemination.

The first part of the study dealing with stratocumulus clouds is complete and the results form the technical portion of this report. A manuscript that has recently been prepared covering this subject is attached as an Appendix. The abstract describes the key finding that cloudy mean LWP is invariant with cloud fraction for cloud cover between 20% - 80%. With reference to the Appendix, this is shown in Figures 7a and 7b which are based on LANDSAT data. Similar conclusions are reached with ISCCP data shown in Figures 9 and 10. This has important implications for General Circulation Models. A possible application is described in the Discussion section of the Appendix. We can basically use an idea that has been proposed for dealing with GCM hydrology. Efforts are being initiated along this direction with the Goddard GCM developed by Dr. Yogesh Sud. We have collaborated with Dr. Bruce Wielicki of NASA Langley in this effort. The material will be presented at the Eighth AMS Radiation Conference in Nashville, TN in January 1994 and is expected to be published during calendar year 1994.

During the next grant year, results from the latter part of Ms. Ginger's thesis will be prepared for publication. A preview of the results may be seen in the thesis which is being mailed separately. As per our original research proposal, a model of the small scale liquid water path distribution will be solved for the radiation field which will be compared with ERBE data which is at coarser resolution. We also intend to corroborate the LWP distributions found in our study with SSM/I data which will be made available to us by Dr. Grant Petty of our department. The level of effort that was requested originally has not changed.

Graduate students supported:

Kathryn Ginger (M.S., Dec. 1993)
Jaya R. Rao (joined group in June 1993)

APPENDIX

The Interpretation of Remotely Sensed Cloud Properties From a Model Parameterization Perspective

Harshvardhan[1]
Bruce A. Wielicki[2]
Kathryn M. Ginger[1]

[1]*Department of Earth and Atmospheric Sciences*
Purdue University
West Lafayette, Indiana

[2]*Atmospheric Sciences Division*
NASA Langley Research Center
Hampton, Virginia

Abstract

A study has been made of the relationship between mean cloud radiative properties and cloud fraction in stratocumulus cloud systems. The analysis is of several LANDSAT images and three-hourly ISCCP C-1 data during daylight hours for two grid boxes covering an area typical of a general circulation model (GCM) grid increment. Cloud properties were inferred from the LANDSAT images using two thresholds and several pixel resolutions ranging from roughly 1/16 km to 8 km. At the finest resolution, the analysis shows that mean cloud optical depth (or liquid water path) increases somewhat with increasing cloud fraction upto 20% cloud coverage. More striking, however, is the lack of correlation between the two quantities for cloud fractions between roughly 0.2 and 0.9. When the scene is essentially overcast, the mean cloud optical depth tends to be higher. Coarse resolution LANDSAT analysis and the ISCCP 8 km data show lack of correlation between mean cloud optical depth and cloud fraction for coverage less than about 95%.

This study shows that there is perhaps a local mean liquid water path (LWP) associated with partly cloudy areas of O (100 km). A method has been suggested to use this property to obtain the cloud fraction in a GCM when the model computes a grid box mean LWP.

1. Introduction

The role of clouds in modifying the earth's radiation budget has never been doubted. In recent years, there has been the realization that climate simulations will not gain widespread acceptability as long as there are nagging doubts related to the manner in which clouds are treated in these models. An appreciation of the current status may be gained from the comprehensive study made by Cess et al. (1990) who attributed most of the differences in the radiative response of nineteen general circulation models to differences in their cloud parameterization. These models had been forced with an imposed positive and negative uniform change in sea surface temperature, a forcing that acted as a surrogate for the anticipated radiative forcing produced by changes in the concentration of radiatively active atmospheric constituents.

Concern with this weak element in present climate models has led to the identification of the role of clouds in atmospheric and hydrologic systems as the area of scientific study of the highest priority (Committee on Earth Sciences, 1989). Current research includes the cataloging and interpretation of global cloudiness data in the International Satellite Cloud Climatology Project (ISCCP, Rossow and Schiffer, 1991) and parallel field observations (Cox et al., 1987). It is felt that the analysis of data from global and regional studies will help to formulate improved cloud generation and radiative parameterization schemes in numerical atmospheric models. However, in order to assimilate observational results, it is first necessary to set up a framework for the interpretation of cloud data presented to modelers. This is necessary because observational results are obtained through an inversion process based on several assumptions, some quite reasonable, but others primarily for the sake of expedience. Models, on the other hand, compute radiative fields directly, using given constituent properties and thermodynamic fields under the assumption that the atmosphere is stratified into horizontally homogeneous layers occupying a defined area.

This study is devoted to the interpretation of information related to cloud fields that can be directly used in numerical models. We have restricted ourselves to selected regions and cloud formations and to only two sources of information. These are the analysis of LANDSAT images

of stratocumulus (Wielicki and Welch, 1986) and ISCCP data from the stratus area off the west coast of North America. The area of the LANDSAT images analyzed is 58 km on a side, comparable to the grid increment of three dimensional mesoscale models while ISCCP cloud statistics are for a 2.5° x 2.5° latitude-longitude area which is typical of the spatial scale of global general circulation models (Giorgi and Mearns, 1991). Further, we are confining ourselves to day time observations of visible reflectance since these provide a first order estimate of optical thickness. Even this limited sample reveals the necessity of establishing some ground rules for the meaningful application of satellite cloud data to atmospheric radiation models. Section 2 introduces the nomenclature used in the study, in particular a definition of cloud fraction that is appropriate for the direct computation of radiation fields in climate models. Section 3 is an analysis of an ensemble of LANDSAT images of stratocumulus clouds within the framework defined in Section 2. Section 4 extends the analysis using ISCCP data for stratocumulus cloud fields. Section 5 summarizes the results and discusses the implications for cloud modeling.

2. Cloud Properties

Inspection of visible images of the earth from space show that cloudiness is ubiquitous. Cloudy areas stand out in contrast to the generally darker background, particularly over oceanic areas. Images constructed from thermal emission in the atmospheric window also reveal cloudiness through the temperature difference between cloud tops and the usually warmer surface. Quantitative analysis generally begins with a procedure to discriminate cloudy areas from the background clear areas. The fraction of an arbitrary horizontal area determined to be cloud covered is the cloud fraction. Further processing can provide information on the optical properties of the clouds identified in the prior step. Unfortunately there are no unambiguous and universal rules that can be followed to identify cloudy areas and ascribe optical properties to them. This is a consequence of the rich horizontal variability of cloudiness at all scales compounded by the presence of geometric structure.

Nevertheless, in order to transfer information obtained from the analysis of remotely sensed observations into a cloud-radiation scheme to be used in an atmospheric model, it is

necessary to create a discrete model of cloudiness. This may be appreciated by considering the manner in which the presence of clouds is determined in current three dimensional atmospheric models. Generally, two classes of clouds are formed: stratiform clouds and convective clouds. The former are generated by a super saturation criterion in the grid box and the latter through a convective parameterization. The relative humidity threshold for the presence of super saturated clouds could be 100% (Randall et al., 1989) or some lesser value which is incorporated in a fractional cloud cover algorithm (Slingo, 1987). There are numerous different schemes for the diagnosis of convective clouds. In addition to the determination of the presence of clouds, models are now assigning optical properties to the generated clouds usually in a diagnostic sense using empirical relations involving temperature, cloud water or altitude. A tabulation of cloud generation techniques and optical thickness schemes incorporated in current general circulation models (GCMs) is provided in Cess et al. (1990).

The radiative fluxes within the atmosphere and net flux at the boundaries for each model grid point are computed from the cloud cover, cloud optical properties and the temperature and gaseous constituent profile. The information necessary to compute radiative fluxes is provided only at a spatial scale corresponding to the grid increment of the model, Δx, which is typically 100-500 km. The atmospheric column within these boundaries is allowed to be clear or covered by extensive clouds over a prescribed fractional area (including complete overcast corresponding to a cloud fraction of 1.0). In the model envisaged here, the horizontal area representing the numerical model grid is considered to be subdivided into areas of side, Δp, which will be called the pixel size or resolution. It should be noted in passing that the grid increment of GCMs is also referred to as the model resolution, perhaps erroneously (Pielke, 1991). The distinction between pixel resolution and model grid increment should be kept in mind as it is central to the framework of this study.

We now state that a pixel is allowed to be clear or cloudy but not partly cloudy, and if cloudy, consists of a column of non-zero optical thickness. The model grid of side Δx then contains several pixels which are clear or cloudy. The ratio of cloudy to total number of pixels is

defined as the cloud fraction of the model grid. It will be further assumed that the individual pixels contribute independently to the radiation flux at any vertical level of the model grid. Cahalan et al. (1993) have shown that this is a justifiable assumption for marine boundary layer clouds. The definition of cloud fraction presented here is energy conserving at any pixel resolution and more importantly directly applicable to GCM radiation computations. Unfortunately, attempts at inverting the reflected radiance field to fit this scheme are confounded by the nature of cloudiness (Schertzer and Lovejoy 1987; Cahalan and Joseph, 1989) which exhibits variability at all length scales. As a consequence, the pixel size and reflectance threshold above background used to discriminate clouds will determine the cloud fraction and pixel reflectances of a particular image (Wielicki and Welch, 1986; Wielicki and Parker, 1992; Chang and Coakley, 1993). However, the distribution of reflectances when averaged over the image and the contribution of the areas designated clear provides the grid mean radiative property required by modelers.

A further consideration is the difference in temporal scale between satellite images,which provide essentially instantaneous fields of cloudiness and GCMs in which cloud fields are updated at intervals ranging from one to twelve hours. In some models, the radiation field is held fixed within these time intervals even though thermodynamic fields are allowed to change. The time scale is much longer than that associated with turbulent processes within clouds and even the life cycle of individual cells embedded within cloud fields. Again, what is required is a statistical description of the radiative properties of the pixels contained within the GCM grid averaged over the time interval between cloud diagnosis updates.

Once we have established the ground rules stated above, a statistical description of cloudiness can be formulated. The usual statistical model of cloudiness describes the frequency of occurrence of various classes of sky cover and is built up from conventional meteorological observations. These models can also be extended to apply to horizontal scales that are larger or smaller than the observations (Falls, 1974; Henderson-Sellers and McGuffie, 1991). Application of these cloud models to global sampling strategies has focused primarily on cloud amount

(Hughes and Henderson-Sellers, 1983; Rossow, 1989), which by itself is not sufficient to describe the radiative properties of the area under consideration. Now that global estimates of cloud optical properties are available from ISCCP (Rossow and Schiffer, 1991), a model of cloudiness more appropriate for GCM applications is possible.

A particularly simple model analogous to those used in hydrology (Entekhabi and Eagleson, 1989) considers the GCM grid area average radiative property, say the planar albedo, A, to be the expectation of that property, E(A). The model is illustrated for the total atmospheric column but in principle can be applied to a particular layer as well. Following Stephens (1988) and Rossow (1989), it will be assumed that the atmospheric column contained in the horizontal area $(\Delta x)^2$ as viewed from the top of the atmosphere is composed of variable column amounts of liquid water and also a region where the presence of condensate can not be detected by the applied threshold criterion (the clear region). For simplicity, let us assume that the clear area has zero albedo and that the cloudy portion consists of several pixels of area $(\Delta p)^2$ whose individual radiative properties can be measured from a remote sensing system. If Q Watts of radiant energy is reflected by the entire grid of area $(\Delta x)^2$, then

$$E(A) = \frac{Q}{\mu_0 S_0 (\Delta x)^2} \tag{1}$$

where μ_0 is the solar zenith angle, S_0 is the solar constant and E(A) is the expectation or grid area averaged planar albedo. If a fraction, C, of the total number of pixels is cloudy, then the mean albedo of the cloudy pixels is E(A)/C and the pixel albedos may be represented by a distribution f(A). For example, the study of fair weather cumulus clouds by Wielicki and Welch (1986) suggests an exponential distribution of the form

$$f(A) = \frac{C}{E(A)} exp\left[-\frac{C\,A}{E(A)}\right], \quad A > 0. \tag{2}$$

When (2) is to be applied to a satellite image it is understood that A should be greater than some non-zero threshold for discriminating clouds from the background and that C will depend on this threshold. In general, for an arbitrary area $(\Delta x)^2$, the quantities C, E(A) and the distribution f(A)

will vary from one instant to another and at a particular time these quantities will vary from location to location depending on the cloud field. Moreover, these quantities will also be different when the averaging area $(\Delta x)^2$ is changed or the pixel size, Δp, is changed. In this study the radiative properties considered are the nadir reflectance measured by the LANDSAT family of satellites, and the effective spherical albedo from ISCCP.

In the analyses that will follow, cloud fraction and area mean cloud radiative (and optical) properties will be obtained using different thresholds and pixel resolutions. These will be compared to 'reference' properties which are obtained using the bispectral threshold and the highest resolution available. The differences are at times referred to as 'errors' but it should be understood that the 'reference' measurements are not absolute but are defined within the constraints of the assumption that the pixel is completely full of cloud of constant optical depth. Even for the highest resolution data available this is not strictly true.

3. LANDSAT Analysis

Wielicki and Parker (1992), hereafter denoted WP, showed that threshold cloud retrieval methods similar to ISCCP are subject to two primary error sources: an underestimation of the amount of optically thin cloud, which cannot be detected by the threshold, and an overestimation of cloud amount caused by triggering the threshold with partially cloud filled fields of view. The former effect dominates for cirrus and both are important for oceanic boundary layer cloud (WP).

The study by WP, however, did not consider derived cloud reflectance or cloud optical depth. The consequences of using different thresholds and resolutions are summarized schematically in Figure 1 which is illustrated for measurements of nadir reflectance. It may be noted that the two lowest panels show the same cloud fraction (25%) but the cloud reflectance and inferred optical depth at high resolution may exceed the low resolution value by a considerable amount. These differences will tend to increase as the regional cloud fraction decreases. Because of these uncertainties, we will use the high spatial resolution LANDSAT data

to check the accuracy of simulated ISCCP results for cloud reflectance and optical depth and to corroborate any conclusions drawn from ISCCP results.

The LANDSAT Thematic Mapper (TM) instrument flew on the LANDSAT 4 and LANDSAT 5 spacecraft. The TM has seven narrow spectral bands with central wavelengths of 0.48, 0.56, 0.66, 0.83, 1.65, 2.21, and 11.5 μm. The six solar reflectance bands have a field of view of 28.5 meters, while the 11.5-μm band has a field of view of 114 meters. All seven bands are atmospheric windows (i.e., small absorption by atmospheric gases).

As in WP, we selected the 0.83-μm and 11.5-μm spectral bands as similar to those available on meteorological satellite instruments such as the VAS (VISSR Atmospheric Sounder) imager on the GOES (Geostationary Operational Environmental Satellite) satellites and the AVHRR (Advanced Very High Resolution Radiometer) imager on the polar orbiting satellites. These near-visible and infrared window channels are similar to those used for the majority of satellite cloud retrieval algorithms, including the ISCCP (Coakley and Bretheron, 1982; Minnis et al., 1987; Rossow et al., 1985). While the 0.66-μm band would be a closer match to the GOES visible spectral band, the 0.83-μm band was selected because of its greater dynamic range and lower ocean surface reflectance.

The reference cloud cover defined for this study is determined using a bispectral threshold method similar to ISCCP on 57 meter resolution LANDSAT data. For convenience, 57-meter resolution data will henceforth be referred to as 1/16 km resolution data. The 114-meter resolution 11.5-μm band data are replicated to provide bispectral data at 57-meter spatial resolution. The replication of the 11.5-μm data has little or no impact on the results since the clouds most sensitive to spatial resolution are found to be cumulus and stratocumulus. These boundary layer clouds are detected almost exclusively by the 0.83-μm channel. The reference cloud cover uses a nadir reflectance threshold $R_t = R_{clr} + \Delta R$ and a brightness temperature threshold $T_t = T_{clr} - \Delta T$, where R_{clr} is the nadir clear-sky reflectance and T_{clr} is the clear-sky

brightness temperature. Nadir reflectance is calculated as an equivalent Lambertian reflectance (Wielicki and Welch, 1986),

$$R = \frac{\pi I}{\mu_0 S_0}, \tag{3}$$

where I is the nadir radiance. With this definition, a perfect Lambert reflector would have a nadir reflectance of 1.0. Calibration coefficients for the LANDSAT spectral bands are taken from Salomonson and Barker (1987) and Markham and Barker (1986). The actual reference thresholds vary as the background variability of the clear ocean increases or decreases. For the 45 cloud fields used in the present study, ΔR has an average value of 0.017 and a standard deviation of 0.008. Corresponding values for ΔT are -1.5K and 0.6K. These values are within 0.001 and 0.1K of those found in WP. Estimated rms error in the reference cloud fraction is less than 0.05, and an error analysis can be found in WP.

The location and time of observation of the 45 scenes is listed in Table 1. The selected scenes are typical of the variety of boundary layer clouds expected in the subtropics, ranging from trade cumulus to solid stratocumulus decks. They were selected from browse images to obtain a wide range of cellular structures: open/closed, cloud cell diameters from 0.5 to 50 km, and cloud streets. After applying the LANDSAT threshold (LS) and the somewhat more stringent ISCCP threshold (IS) separately on each scene, the cloud fraction and cloud pixel mean nadir reflectance have been computed and are shown as a scatter plot in Figs. 2(a) and (b). In addition, the data in Fig. 2(a) are listed in Table 1 so that each point on the plot may be identified with the particular scene. As in the ISCCP C1 data, the average is over the cloudy pixels alone such that, with reference to Figure 1, the mean is of I_1, I_2, ... for each pixel identified as cloudy by the particular threshold. The general pattern is not influenced greatly by choice of threshold. For cloud fractions less than 0.2, the mean nadir reflectance increases with cloud fraction. There is then a wide range of cloud fraction over which there appears to be little correlation between reflectance and cloud fraction. Completely cloud filled scenes, however, tend to have the highest values of mean reflectance although there are exceptions to this rule. The most obvious is scene 11 which

is roughly 40% cloudy but has highly reflective clouds. This is a scene of cloud cover following a cold air outbreak in which the larger LANDSAT image shows essentially clear skies over half the image and a very thick unbroken deck over the rest of the scene.

When the same scenes are analyzed at progressively coarser resolution but using the same threshold, there is a marked evolution in the pattern. This is shown in Figs 3(a) - (d) which shows a series of scatter plots of analyses at 1/16, 1/2, 2 and 8-km resolution respectively using the ISCCP (IS) threshold. Figure 2(b) and Figure 3(a) are identical with the other panels showing the effect of coarsening the resolution. Figure 3(d), which may be considered to be simulated ISCCP data shows that mean nadir reflectance and cloud fraction are uncorrelated at least out to a cloud fraction of 0.8.

The effect of coarsening the resolution and changing from LS to IS threshold is summarized in Figures 4(a) and (b). As mentioned in WP, the coarser resolution analysis overestimates cloud fraction except for scenes with small amounts of scattered clouds. For these cases, the resolution results in the larger pixels being classified as clear. An extreme example is scene 17 which has a cloud fraction of 0.11 at 1/16-km resolution and using the LS threshold but is classified as completely clear at the 8-km resolution using the ISCCP threshold. However, it is important to realize that changes in cloud fraction are accompanied by concomitant changes in mean nadir reflectance.

In order to examine the implications of the patterns exhibited in the panels of Figs. 2 and 3 it is necessary to present the data in terms of a physical quantity such as the optical depth or cloud liquid water path. This is accomplished by the following procedure. For each cloud pixel, the small contribution of the ocean surface reflectance is first removed following the method of Platt et al. (1980). The remaining cloud reflectance is then compared to a look-up table to convert nadir reflectance into an estimate of cloud optical depth at 0.83 μm. The look up table is based on radiative transfer calculations using a multiple scattering finite difference model (Barkstrom, 1976; Suttles, 1981), which has been checked for consistency against the adding doubling approach used by ISCCP. Single scattering properties are derived using Mie calculations for a

size distribution of water droplets with an effective radius r_e of 10 μm and a variance of 0.10, consistent with ISCCP (Rossow et al., 1991). Figure 5 shows the resulting reflectance at nadir as a function of cloud optical depth for solar zenith angles of 25, 45 and 60 degrees, covering the range of values used in this study. A more complete description of the radiative calculations can be found in Wielicki et al. (1990). Finally, an estimate of cloud liquid water path (LWP) is made by using the following relationship (Stephens, 1984),

$$LWP = \frac{2}{3} \tau r_e \tag{4}$$

where τ is the optical depth and r_e is the effective particle radius.

A linear average of the pixel optical depth or LWP of the cloudy pixels alone is then a measure of the amount of liquid in the region. This process was first carried out at the highest resolution using the LS threshold. After estimating the above parameters for the LANDSAT full resolution data we then spatially averaged the LANDSAT radiance data to a spatial resolution of 7.2 km, approximating the ISCCP GOES data source. As in WP, we then applied the ISCCP cloud detection thresholds to the spatially averaged data, and computed ISCCP estimates of cloud reflectance, cloud optical depth, and cloud LWP.

As mentioned earlier, estimates of mean reflectance are influenced by resolution and threshold. This of course carries over to estimates of the optical depth. Figure 6 is a comparison of the linearly averaged optical depth for the 45 scenes at two resolution and using the LS and IS thresholds. The coarse resolution analysis underestimates the optical depth for partly cloud scenes. This underestimate could be substantial.

The inferred mean LWP for the scenes is presented in Fig. 7(a) and (b) as a function of the regional cloud fraction. The IS threshold has been used since further analysis is based on ISCCP data. Table 1 lists these quantities for each of the 45 scenes. Some features of Fig. 2(b) are evident in Fig. 7(a). There is some correlation between mean LWP and cloud fraction for small values of the cloud fraction. There is then little discernible correlation, although overcast scenes tend to have the highest mean LWPs.

Fig. 7 (b) shows a pattern similar to Fig. 3(d) in that there appears to be little correlation between mean LWP and cloud fraction for partly cloudy scenes. This suggests that when scales of variability less than O (10 km) are averaged out, the mean liquid water path in partially cloudy stratus cloud fields is essentially independent of the cloud fraction. Since the total volume of liquid in the region is the product of mean LWP (in appropriate units) and the area covered by clouds, the total volume and also the mass loading per unit area of the entire region is a linear function of the cloud fraction. The implications of this are discussed later following an analysis of ISCCP data.

4. ISCCP Analysis

While LANDSAT data are well suited for testing the sensitivity to spatial resolution, the data are about 30 times as expensive to acquire and process as GOES or AVHRR data. This expense limited the scope of the present study to an examination of 45 oceanic cloud fields, each 58.4-km square. More extensive analysis must rely on coarse resolution global data such as that cataloged in the ISCCP C1 data set (Rossow and Schiffer, 1991).

We have restricted ourselves to one region and type of cloud in this study. In order to correspond most closely with the LANDSAT study, we have chosen two areas off the west coast of N. America during the month of July 1987. This time period coincides with the FIRE campaign (Cox et al., 1987) conducted in the same region. Figure 8 shows the location of the two 2.5° lat. × 2.5° long. grid boxes chosen for the analysis of ISCCP C1 data.

The contours show the monthly mean planetary albedo from the Earth Radiation Budget Experiment scanner data (Harrison et al., 1990). The choice of areas was partly determined by the availability of the most complete ISCCP C1 data on cloud properties. Other grid boxes tended to have missing data. Box A is at the edge of the stratus region and tended to be partly cloudy throughout the month while Box B was partly cloudy or completely overcast during this period (Kloesel et al., 1988).

Unlike the LANDSAT analysis, the data used here is for the same region but at three-hourly intervals during daylight hours. As in the previous analysis, cloud fraction at the 8 km

nominal resolution is one of the variables considered. An estimate of the mean radiative properties of the cloudy pixels is the parameter TAU cataloged in the C1 data. Details of the procedure used to obtain TAU are in Rossow et al. (1991). It will suffice here to mention that the processing is quite similar to the LANDSAT reduction described earlier, except that bi-directional reflectances are used in the table look up instead of the nadir reflectance given by Fig. 5. Also, the mean TAU for the scene is not a linear average of retrieved TAUs for each pixel but an energy weighted average. This is accomplished by first converting TAU to a spherical albedo before pixel averaging is performed.

Figs. 9 and 10 show the scatter plot of the mean spherical albedo of the cloudy pixels in the scene as a function of the cloud fraction for boxes A and B respectively. There are over one hundred realizations presented in the plots. During the whole month, the entire scene was never completely clear for either of the two grid boxes.

During each day, points represent scenes separated by only three hours temporally. In order to examine the degree to which cloud cover and optical properties change over that short span, we have identified each day of the month with a character starting with A for July 1 and continuing with B for July 2 and so on. The character α represents data for July 27, β is for July 28, etc. With the exception of overcast days in box B, it appears that the three-hour period is sufficient for the cloud scene to change appreciably.

The similarities between Figs. 9 and 10 and Fig. 3(d) are striking. Although the mean radiative property considered is somewhat different, both the nadir reflectance and spherical albedo act as proxies for the optical depth of the cloudy pixels. Unfortunately, at present, a linear weighted average liquid water path is not available in the ISCCP C1 data so a plot such as shown in Fig. 7(b) can not be presented.

However, with the information available, the scene-averaged properties of boxes A and B tend to confirm the conclusions drawn from the LANDSAT analysis. At the resolution considered here, there is no correlation between mean cloud radiative properties and cloud fraction for partly cloudy scenes that are about 200 km on a side, at least for cloud fraction less

than about 0.8. The data for box B does show a tendency for cloudier scenes to be optically thicker on average when the cloud fraction exceeds 0.8. The highest mean albedos are for the overcast scenes.

5. Discussion

The study described above, though limited, suggests a direction in which cloud parameterizations could embark on. For low level single layer clouds, in particular maritime stratus, the mean liquid water path, hence optical depth, of the cloudy areas in a grid box is essentially invariant with cloud fraction. This appears to hold quite well for cloud fractions between 0.2 and 0.8. The total volume of liquid in the box is therefore a linear function of cloud fraction. This sort of relationship has been observed in a two-dimensional cloud ensemble model for the lowest model layer (Xu and Randall, 1992). Of greater relevance here, is the recent application of such a relationship to the modeling of surface hydrology in a GCM.

There are some parallels between the problems involved with the parameterization of cloud radiative properties and surface hydrology in GCMs. Diagnostic or prognostic variables in GCMs are defined for the entire grid box which is typically a hundred or so kilometers on a side. Thus the precipitation rate or liquid water amount computed at any time step is an average value over the entire grid box, i.e. the expectation, E(R), of the variable R. The fate of precipitation falling on the surface of the model grid box, however, depends on the local precipitation rate. Interception, infiltration and run-off are all non-linear functions of this local rate (Entekhabi and Eagleson, 1989). Likewise, the radiative properties of the grid box, such as albedo and emittance depends crucially on the distribution of the liquid water path, not simply on the area averaged value (Harshvardhan and Randall, 1985). A first order approximation to the subgrid scale variability can be obtained by estimating the cloud fraction (or wetted area for rainfall) and mean cloud properties (or mean precipitation rate) of the cloudy (precipitating) area. Our study shows that this may be accomplished in the following manner.

Kedem et al. (1990) and others have shown that there is a linear relationship between rainfall volume and fractional area of rain in convective systems. This implies that the mean

rainfall rate where it is raining is unique to the rainfall climatology of the location. This has been explained on purely statistical grounds but seems plausible. Recently, Eltahir and Bras (1993) have used this idea to estimate the fractional coverage of rainfall within a GCM grid box by using station data for the local mean rain rate and GCM output of grid-mean rain rate.

Our stratus study has shown that there is perhaps a local mean liquid water path associated with partly cloudy areas of O (100 km). As with convective rainfall, it appears that at any instant the mean LWP of the cloudy area is the average of a population that does not change with change in cloud fraction, at least over the range 0.2 - 0.8. In effect, for an area the size of a GCM grid, there is a distribution of LWP which does not change appreciably. A simple model of such a cloud field is that proposed by Coakley (1991): a stratus deck is composed of cells of O (1 km) which tend to be optically thicker in the center and somewhat thinner at the edges. What appears to be a cloudy region is actually an array of such cells, each with somewhat different LWP distributions. For the region as a whole, the distribution could be of the form given by Eq. (2). Over the parameter space that this conjecture is valid, one could then estimate the cloud fraction based on some knowledge of the mean LWP within the cloudy portion of the box.

There is, of course, a serious limitation to the application of this idea. Whereas local mean rain rate is known from station data, there is no corresponding history of cloud LWP observations, at least not on the global scale necessary. One possibility is to compute directly the mean LWP for cloudy areas based on empiricism or a cloud physics process model. After all, GCMs that use relationships between cloud temperature and LWP (Cess et al., 1990) are relying on an empirical relationship.

The computation of a cloud fraction independently of the GCM liquid water computation will introduce a degree of flexibility not yet incorporated in current models. For instance, it will be possible to differentiate between the grid mean radiative properties of open-cell and closed-cell convection which are known to occur under different climatological conditions (Agee, 1987). A climate change experiment could then include a cloud fraction feedback which may not be trivial

since, for thick clouds, grid mean radiative properties are much more sensitive to cloud fraction than to optical depth.

Acknowledgements. This study was supported in part by NASA Grant NAGW-3150. The authors are grateful to Lindsay Parker for programming assistance, Tim Gilbert for the graphics and Wanda Curtis for typing the manuscript.

References

Agee, E.M., 1987: Mesoscale cellular convection over the oceans. *Dyn. Atmos. Oceans*, **10**, 317-341.

Barkstrom, B.R., 1976: A finite difference method of solving anisotropic scattering problems. *J. Quant. Spectrosc. Radiat. Trans.*, **16**, 725-739.

Cahalan, R.F., and J.H. Joseph, 1989: Fractal statistics of cloud fields. *Mon. Wea. Rev.*, **117**, 261-272.

Cahalan, R.F., W. Ridgway, W.J. Wiscombe, T.L. Bell, and J.B. Snider, 1993: The albedo of fractal stratocumulus clouds. Submitted to *J. Atmos. Sci.*

Committee on Earth Sciences, 1989: Our Changing Planet: The FY 1990 Research Plan. The U.S. Global Change Research Program. Washington, D.C., 118 pp. plus three appendices.

Cess, R.D., G.L. Potter, J.P. Blanchet, G.J. Boer, A.D. DelGenio, M. Deque, V. Dymnikov, V. Galin, W.L. Gates, S.J. Ghan, J.T. Kiehl, A.A. Lacis, H. Le Treut, Z.-X. Li, X.-Z. Liang, B.J. McAvaney, V.P. Meleshko, J.F.B. Mitchell, J.-J. Morcrette, D.A. Randall, L. Rikus, E. Roeckner, J.F. Royer, U. Schlese, D.A. Sheinin, A. Slingo, A.P. Sokolov, K.E. Taylor, W.M. Washington, R.T. Wetherald, I. Yagai and M.-H. Zhang, 1990: Intercomparison and interpretation of climate feedback processes in 19 atmospheric general circulation models. *J. Geophys. Res.*, **95**, 16,601-16,615.

Chang, F.-L., and J.A. Coakley, Jr., 1993: Estimating errors in fractional cloud cover obtained with infrared threshold methods. *J. Geophys. Res.*, **98**, 8825-8839.

Coakley, J.A., Jr., 1991: Reflectivities of uniform and broken layered clouds. *Tellus*, **43(B)**, 420-443.

Coakley, J.A., Jr., and F.P. Bretherton, 1982: Cloud cover from high resolution scanner data: Detecting and allowing for partially filled fields of view. *J. Geophys. Res.*, **87**, 4917-4932.

Cox, S.K., D.S. McDougal, D.A. Randall and R.A. Schiffer, 1987: FIRE - The First ISCCP Regional Experiment. *Bull. Amer. Meteor. Soc.*, **68**, 114-118.

Eltahir, E.A.B., and R.L. Bras, 1993: Estimation of the fractional coverage of rainfall in climate models. *J. Climate*, **6**, 639-644.

Entekhabi, D., and P.S. Eagleson, 1989: Land surface hydrology parameterization for atmospheric general circulation models including subgrid scale spatial variability. *J. Climate*, **2**, 816-831.

Falls, L.W., 1974: The Beta distribution: a statistical model for world cloud cover. *J. Geophys. Res.*, **79**, 1261-1264.

Giorgi, F., and L.O. Mearns, 1991: Approaches to the simulation of regional climate change: A review. *Rev. Geophys.*, **29**, 191-216.

Harrison, E.F., P. Minnis, B.R. Barkstrom, V. Ramanathan, R.D. Cess and G.G. Gibson, 1990: Seasonal variation of cloud radiative forcing derived from the Earth Radiation Budget Experiment. *J. Geophys. Res.*, **95**, 18,687-18,703.

Harshvardhan, and D.A. Randall, 1985: Comments on 'The parameterization of radiation for numerical weather prediction and climate models'. *Mon. Wea. Rev.*, **113**, 1832-1833.

Henderson-Sellers, A., and K. McGuffie, 1991: An investigation of the Burger distribution to characterize cloudiness. *J. Climate,* **4**, 1181-1209.

Hughes, N.A., and A. Henderson-Sellers, 1983: The effect of spatial and temporal averaging on sampling strategies for cloud amount data. *Bull. Amer. Meteor. Soc.*, **64**, 250-257.

Kedem, B., L.S. Chiu and Z. Karni, 1990: An analysis of the threshold method for measuring area-average rainfall. *J. Appl. Meteor.*, **29**, 3-20.

Kloesel, K.A., B.A. Albrecht and D.P. Wylie, 1988: FIRE marine stratocumulus observations - summary of operations and synoptic conditions. FIRE Technical Report No. 1, Pennsylvania State University, pp. 171.

Markham, B.L., and J.L. Barker, 1986: MSS and TM post-calibration dynamic ranges, exoatmospheric reflectances and at-satellite temperatures, Technical Notes, Aug. 1986, 3-8.

Minnis, P., E.F. Harrison and G.G. Gibson, 1987: Cloud cover over the equatorial eastern Pacific derived from July 1983 International Satellite Cloud Climatology Project data using a hybrid bispectral threshold method. *J. Geophys Res.*, **92**, 4051-4073.

Pielke, R.A., 1991: A recommended specific definition of 'resolution'. *Bull. Amer. Meteor. Soc.*, **72**, 1914.

Platt, C.M.R., D.W. Reynolds and N. L. Abshire, 1980: Satellite and lidar observations of the albeds, emittance, and optical depth of cirrus compared to model calculations. *Mon. Wea. Rev.*, **108**, 195-204.

Randall, D.A., Harshvardhan, D.A. Dazlich and T.G. Corsetti, 1989: Interactions among radiation, convection, and large-scale dynamics in a general circulation model. *J. Atmos. Sci.*, **46**, 1943-1970.

Rossow, W.B., 1989: Measuring cloud properties from space: A review. *J. Climate,* **2**, 201-213.

Rossow, W.B., F. Mosher, E. Kinsella, A. Arking, M. Desbois, E. Harrison, P. Minnis, E. Ruprecht, G. Seze, C. Simmer and E. Smith, 1985: ISCCP cloud algorithm intercomparison. *J. Climate Appl. Meteor.*, **24**, 877-903.

Rossow, W.B., and R.A. Schiffer, 1991. ISCCP Cloud data products. *Bull. Amer. Meteor. Soc.*, **72**, 2-20

Rossow, W.B., L.C. Garder, P.J. Lu and A. Walker, 1991: International Satellite Cloud Climatology Project (ISCCP) Documentation of cloud data. WMO/TD-266, 76 pp., World Meteorol. Organ., Geneva.

Salomonson, V.V., and J.L. Barker, 1987: Recent data quality and Earth science results from the Thematic Mapper. *Adv. Space Res.*, **7**, 217-226.

Schertzer, D., and S. Lovejoy, 1987: Physical modeling and analysis of rain and clouds by anisotropic scaling multiplicative processes. *J. Geophys. Res.*, **92**, 9693-9714.

Slingo, J.M., 1987: The development and verification of a cloud prediction scheme for the ECMWF model. *Quart. J. Roy. Meteor. Soc.*, **113**, 899-927.

Stephens, G.L., 1984: The parameterization of radiation for numerical weather prediction and climate models. *Mon. Wea. Rev.* **112**, 826-867.

Stephens, G.L., 1988: Radiative transfer through arbitrarily shaped optical media. Parts I and II. *J. Atmos. Sci.*, **45**, 1818-1848.

Suttles, J.T., 1981: Anisotropy of solar radiation leaving the earth-atmosphere system, Ph.D. thesis, 180 pp., Old Dominion University, [Available from NTIS, NASA Accession No. N82-32242].

Wielicki, B. A., and R. M. Welch, 1986: Cumulus cloud field properties derived using digital data. *J. Climate Appl. Meteor.*, **25**, 261-276.

Wielicki, B.A., J.T. Suttles, A.J. Heymsfield, R.M. Welch, J.D. Spinhirne, M.C. Wu, D.O'C. Starr, L. Parker and R.F. Arduini, 1990: The 27-28 October 1986 FIRE IFO cirrus case study: Comparison of radiative transfer theory with observations by satellite and aircraft. *Mon. Wea. Rev.*, **118**, 2356-2376.

Wielicki, B.A., and L. Parker, 1992: On the determination of cloud cover from satellite sensors: The effect of sensor spatial resolution. *J. Geophys. Res.*, **97**, 12,799-12,823.

Xu, K.-M., and D.A. Randall, 1992: The semi-empirical basis of a prognostic cloud parameterization for use in climate models. *Proceedings of the 11th International Conference Clouds and Precipitation,* Montreal, Canada, 1144-1147.

Table 1. Identification of the location and time of the 45 LANDSAT scenes analyzed in the study. Also tabulated are the solar zenith angle, cloud fraction and selected cloud pixel mean (CPM) properties at given resolutions for the LANDSAT (LS) and ISCCP (IS) thresholds.

Scene	Date:	Lat / Lon (deg)	Time UTC	Sol Zen (deg)	LS 1/16 Cloud Fraction	LS 1/16 CPM Nadir Reflectance	LS 1/16 CPM Optical Depth	IS 8 Cloud Fraction	IS 8 CPM LWP (mm)
1	6/19/80	N31.60/W117.72	1743	30	0.99	0.43	8.80	1.00	0.054
2	6/21/80	N33.05/W120.18	1754	30	0.99	0.28	4.80	1.00	0.029
3	7/25/80	N31.65/W117.86	1743	33	1.00	0.52	11.20	1.00	0.069
4	7/27/80	N33.08/W120.32	1755	33	0.99	0.29	5.00	1.00	0.031
5	10/23/81	N37.38/W123.03	1807	56	0.99	0.45	10.30	1.00	0.061
6	8/30/82	N31.45/W 79.06	1515	37	0.39	0.22	3.80	0.78	0.011
7	8/30/82	N31.29/W 78.43	1515	37	0.22	0.15	2.00	0.23	0.007
8	10/1/82	N30.28/W128.70	1833	43	0.99	0.34	6.40	1.00	0.035
9	10/8/82	N31.75/W129.90	1839	46	0.99	0.39	7.50	1.00	0.041
10	1/14/83	N26.45/W 79.25	1512	58	0.75	0.42	19.20	0.83	0.077
11	1/14/83	N26.18/W 78.48	1512	58	0.39	0.52	29.20	0.48	0.110
12	8/2/85	N32.73/W121.45	1810	32	1.00	0.62	15.80	1.00	0.103
13	8/11/85	N32.88/W120.87	1804	33	1.00	0.67	18.80	1.00	0.123
14	6/15/87	S 7.22/W115.58	1715	48	0.22	0.18	5.10	0.33	0.012
15	6/30/87	N32.17/W121.00	1800	30	0.93	0.37	8.20	0.97	0.046
16	6/30/87	N31.44/W120.35	1800	30	1.00	0.62	15.90	1.00	0.106
17	7/6/87	N34.57/W122.95	1805	32	0.11	0.07	0.90	0.00	0.000
18	7/7/87	N31.43/W121.88	1806	30	0.17	0.10	1.10	0.09	0.008
19	7/7/87	N32.18/W122.55	1806	30	0.99	0.46	9.10	1.00	0.059
20	7/9/87	N33.62/W119.07	1753	30	1.00	0.63	17.30	1.00	0.113
21	7/9/87	N33.17/W118.64	1753	30	0.98	0.40	8.50	1.00	0.053
22	7/10/87	N33.17/W129.45	1837	30	0.63	0.18	2.90	0.86	0.014
23	7/13/87	S20.03/W 74.59	1426	58	0.79	0.17	3.10	0.89	0.017
24	7/13/87	S20.71/W 74.80	1426	58	0.97	0.27	5.90	1.00	0.031
25	7/14/87	N31.73/W123.66	1812	31	1.00	0.74	23.30	1.00	0.156
26	7/16/87	N31.16/W120.17	1800	31	1.00	0.61	15.30	1.00	0.099
27	7/16/87	N31.73/W120.56	1800	31	1.00	0.72	22.10	1.00	0.148
28	7/23/87	N33.14/W121.81	1806	32	0.29	0.14	1.80	0.47	0.007
29	7/29/87	S20.20/W 75.21	1426	56	0.18	0.13	2.60	0.09	0.011
30	11/18/87	N44.55/W146.07	1950	68	0.36	0.22	10.00	0.45	0.019
31	12/12/87	N14.44/W 67.66	1413	50	0.24	0.13	2.20	0.14	0.007
32	12/31/87	N38.86/W 69.16	1438	69	0.59	0.29	10.80	0.83	0.028
33	3/11/88	N30.27/W 48.42	1310	47	0.27	0.22	4.90	0.36	0.015
34	3/16/88	N33.14/W126.44	1825	47	0.51	0.13	1.80	0.58	0.010
35	4/29/88	N10.11/W138.14	1857	33	0.27	0.22	3.40	0.48	0.011
36	6/22/90	N33.19/W033.80	1218	28	0.87	0.29	6.10	0.95	0.032
37	6/25/90	N33.18/W 16.81	1110	28	0.85	0.55	13.50	0.89	0.080
38	6/30/90	N33.19/W 21.42	1129	28	0.19	0.14	2.40	0.30	0.007
39	7/4/90	N33.19/W 15.26	1104	28	1.00	0.53	12.10	1.00	0.076
40	7/5/90	N36.06/W 25.27	1146	29	0.27	0.21	3.60	0.52	0.010
41	7/5/90	N34.62/W 25.68	1147	29	0.73	0.23	3.80	0.79	0.021
42	7/5/90	N33.18/W 26.08	1147	29	0.95	0.48	14.20	0.95	0.083
43	7/8/90	N33.18/W 33.81	1218	28	0.25	0.31	7.90	0.41	0.022
44	7/10/90	N33.19/W 30.71	1205	29	0.91	0.40	10.80	0.98	0.053
45	7/11/90	N33.19/W 16.81	1110	29	0.80	0.25	3.90	0.94	0.021

FIGURE CAPTIONS

Figure 1. A schematic diagram depicting the role played by threshold and resolution in determining the mean cloud properties of a scene. Insolation is S_0 at a particular zenith angle; the nadir reflectance of each pixel is I_n. Increasing density of the shading depicts increasing reflectance. Unshaded pixels are detected to be clear.

Figure 2. Scatter plot of the mean nadir reflectance of all the cloudy pixels in the scene vs. cloud fraction for LANDSAT images at a nominal resolution of 1/16 km using (a) the LANDSAT (LS) threshold and (b) the ISCCP (IS) threshold.

Figure 3. As in Figure 2 but using the ISCCP (IS) threshold only for resolutions of (a) 1/16 km, (b) 1/2 km, (c) 2 km and (d) 8 km.

Figure 4. Scatter plot of (a) IS – 8 vs. LS – 1/16 cloud fraction and (b) the IS – 8 vs. LS – 1/16 mean nadir reflectance, showing the effects of using different thresholds and resolutions in determining the mean cloud properties of the scene.

Figure 5. Radiative transfer results of the nadir reflectance as a function of the optical depth at three different solar zenith angles for plane parallel homogeneous clouds composed of droplets of effective radius, $r_e = 10$ μm.

Figure 6. Scatter plot of the inferred mean optical depth using the ISCCP threshold at 8 km resolution vs. the same quantity inferred using the LANDSAT threshold at 1/16 km resolution.

Figure 7. Scatter plot of the mean liquid water path (mm) as a function of the cloud fraction derived using the ISCCP threshold (a) at 1/16 km resolution and (b) at 8 km resolution.

Figure 8. The region selected for the ISCCP study. The two grid boxes chosen for the analysis are identified. Contours show the mean planetary albedo for July 1987 as determined by the Earth Radiation Budget Experiment.

Figure 9. Scatter plot of the inferred mean spherical albedo vs. the cloud fraction for daytime images at Box A during the month of July 1987. Characters denote the day of the month. See text for an explanation.

Figure 10. As in Figure 9 but for Box B.

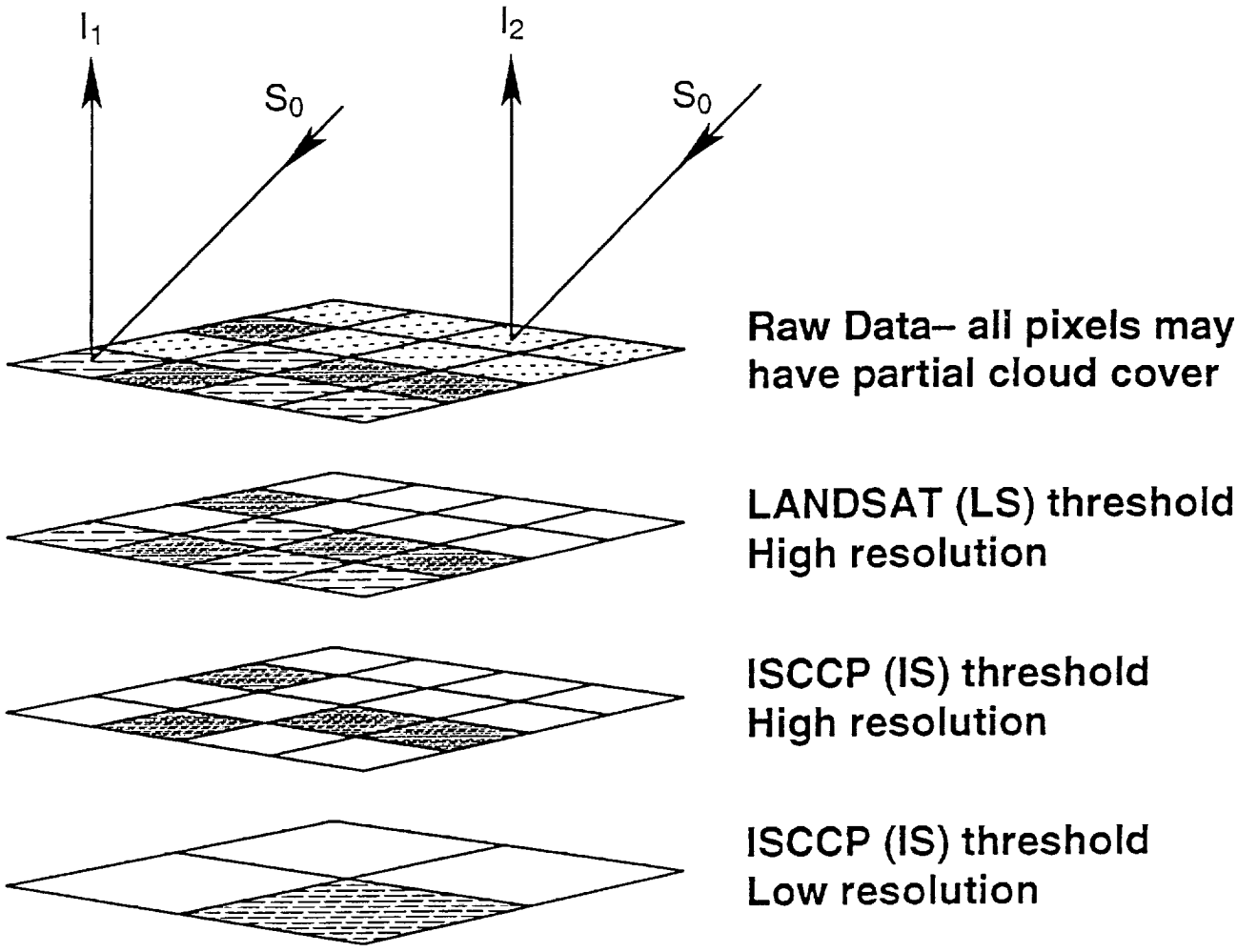
I_1
I_2
S_0
S_0
Raw Data– all pixels may have partial cloud cover
LANDSAT (LS) threshold High resolution
ISCCP (IS) threshold High resolution
ISCCP (IS) threshold Low resolution

Figure 1

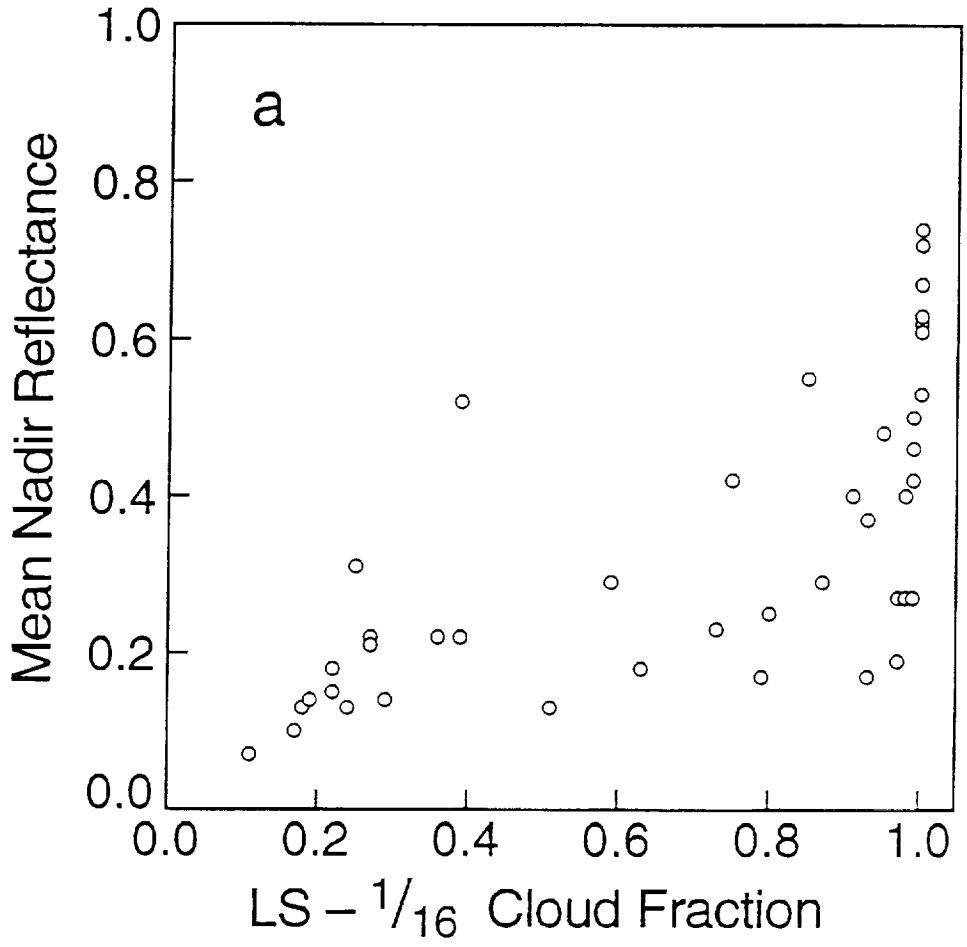
a
Mean Nadir Reflectance
1.0
0.8
0.6
0.4
0.2
0.0
0.0
0.2
0.4
0.6
0.8
1.0
LS – 1/16 Cloud Fraction

Figure 2a

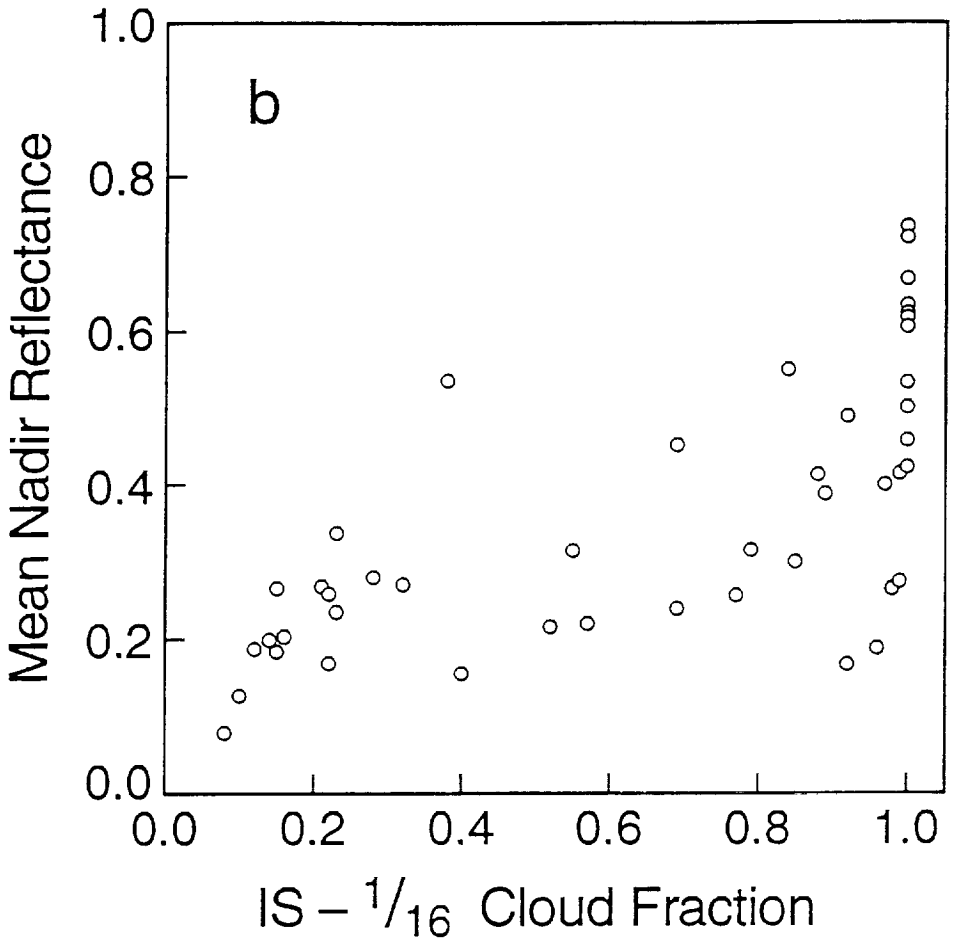
b
Mean Nadir Reflectance
1.0
0.8
0.6
0.4
0.2
0.0
0.0
0.2
0.4
0.6
0.8
1.0
IS – 1/16 Cloud Fraction

Figure 2b

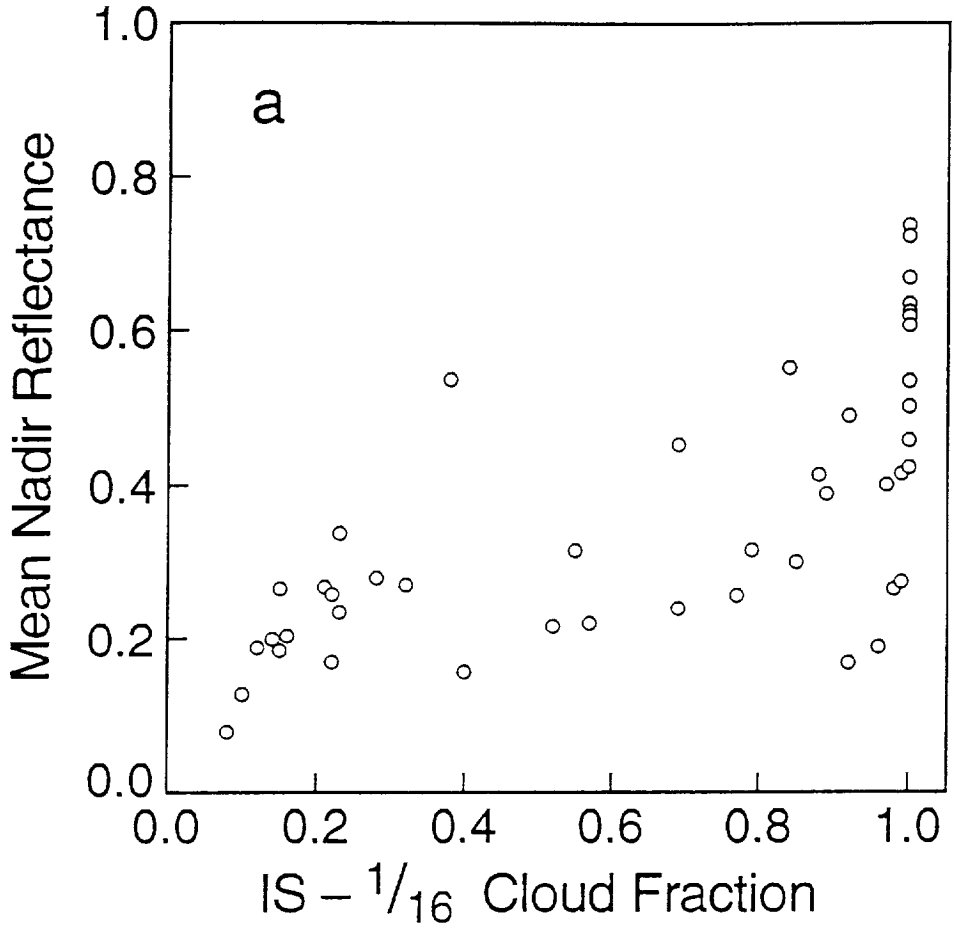
a
Mean Nadir Reflectance
1.0
0.8
0.6
0.4
0.2
0.0
0.0
0.2
0.4
0.6
0.8
1.0
IS – 1/16 Cloud Fraction

Figure 3a

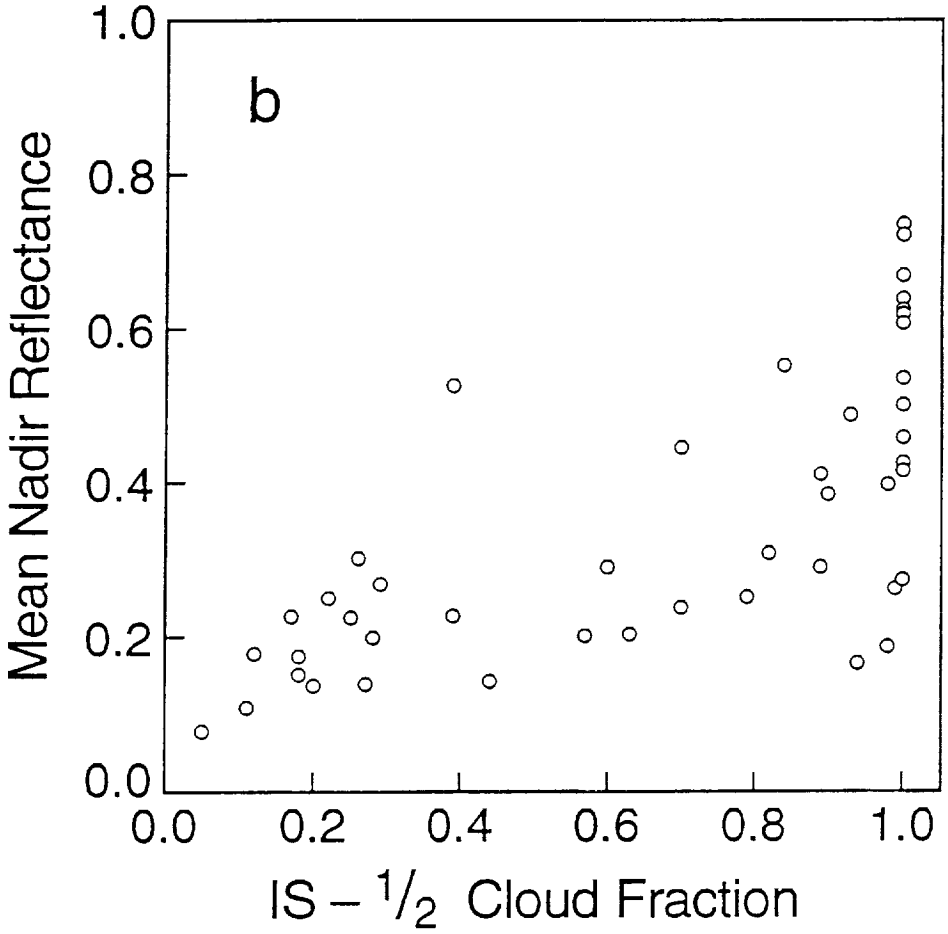
b
Mean Nadir Reflectance
1.0
0.8
0.6
0.4
0.2
0.0
0.0
0.2
0.4
0.6
0.8
1.0
IS – 1/2 Cloud Fraction

Figure 3b

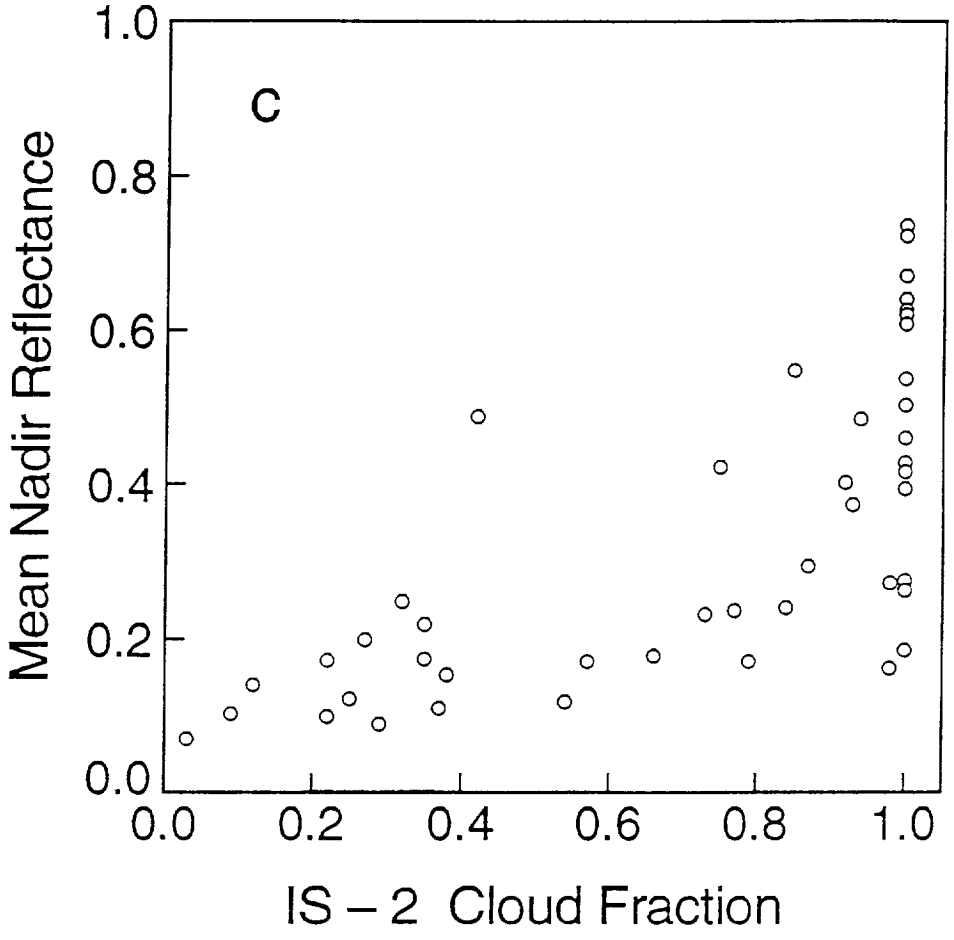

Figure 3c

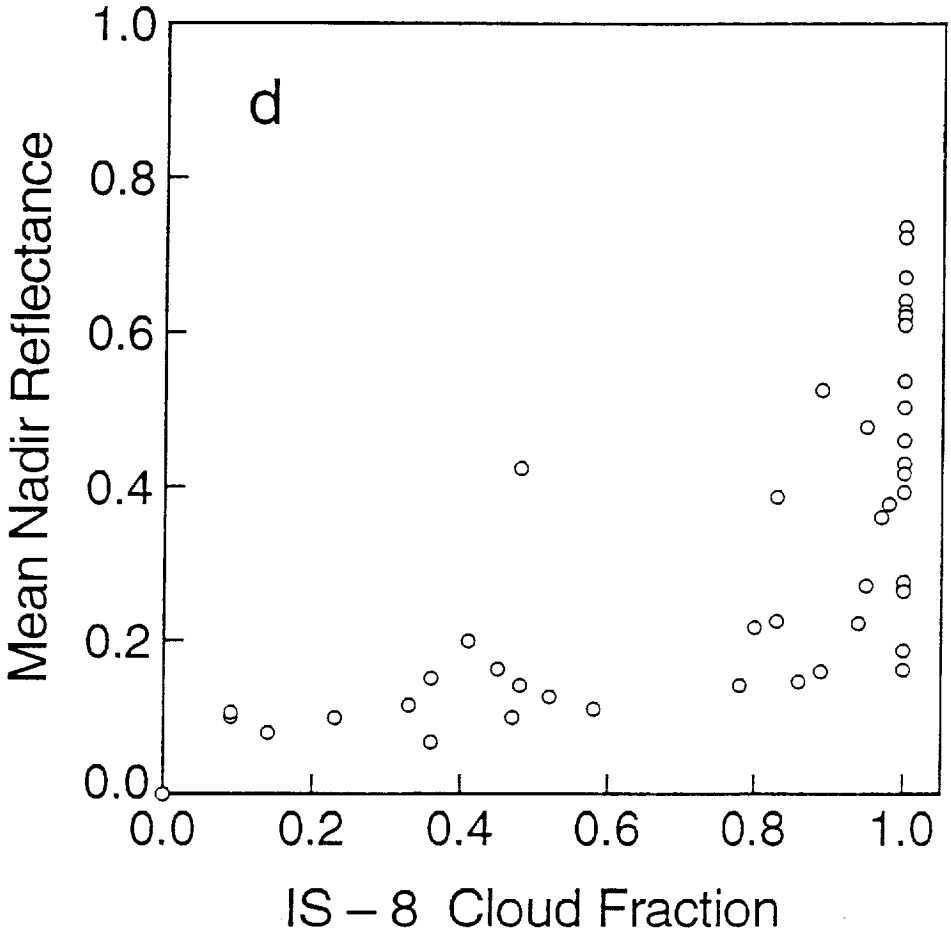
d
Mean Nadir Reflectance
1.0
0.8
0.6
0.4
0.2
0.0
0.0
0.2
0.4
0.6
0.8
1.0
IS – 8 Cloud Fraction

Figure 3d

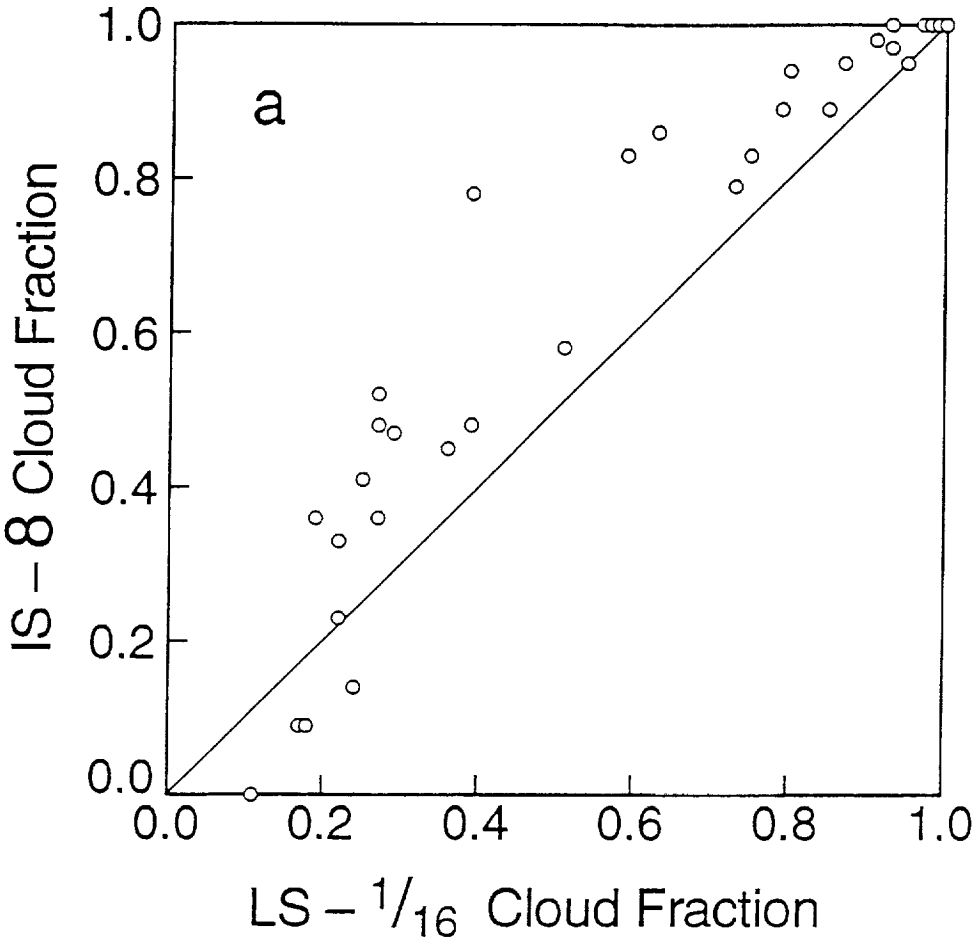
a
1.0
0.8
0.6
0.4
0.2
0.0
0.0
0.2
0.4
0.6
0.8
1.0
IS – 8 Cloud Fraction
LS – 1/16 Cloud Fraction

Figure 4a

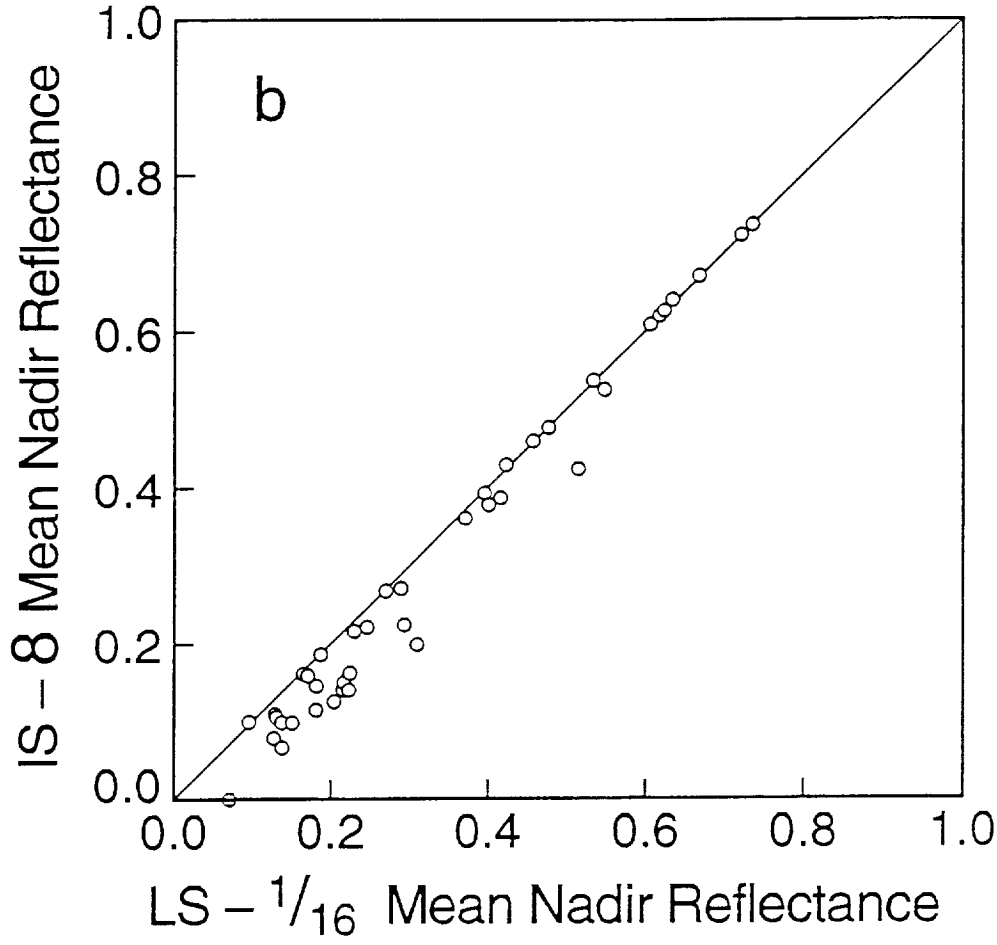
b
1.0
0.8
0.6
0.4
0.2
0.0
0.0
0.2
0.4
0.6
0.8
1.0
IS – 8 Mean Nadir Reflectance
LS – 1/16 Mean Nadir Reflectance

Figure 4b

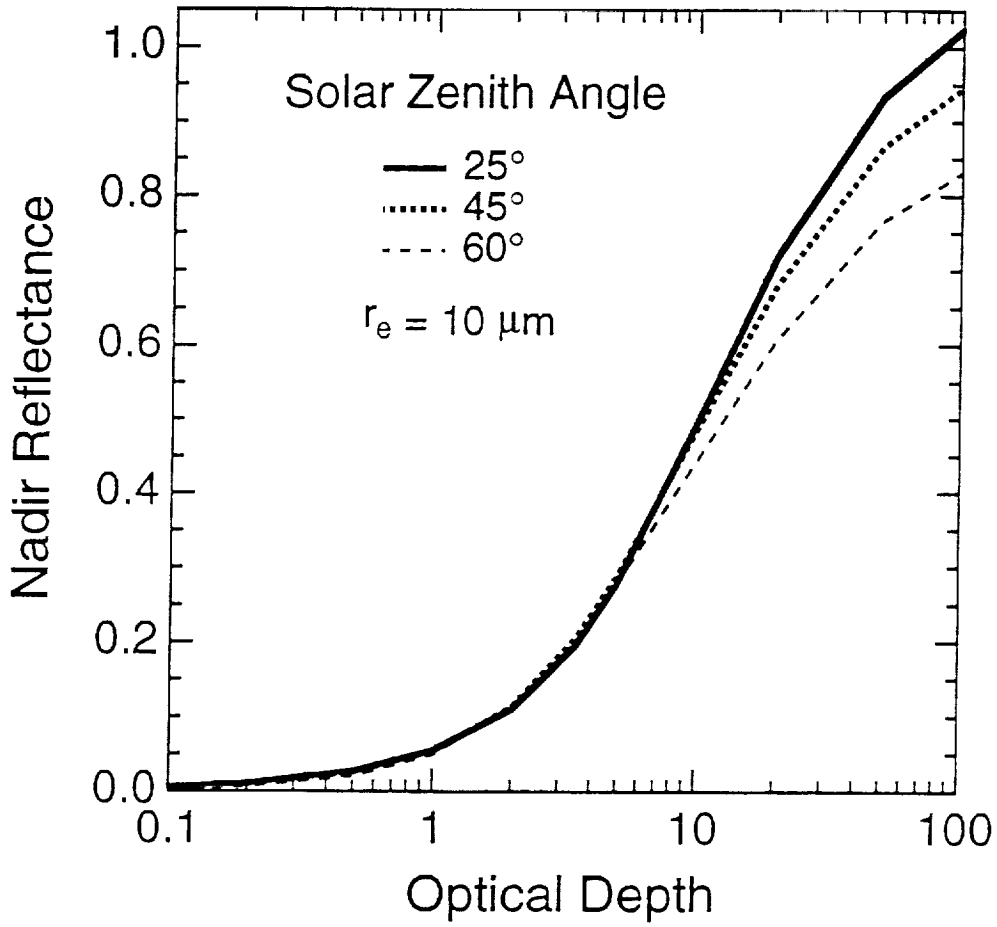
Solar Zenith Angle
25°
45°
60°
r_e = 10 μm
Nadir Reflectance
Optical Depth
1.0
0.8
0.6
0.4
0.2
0.0
0.1
1
10
100

Figure 5

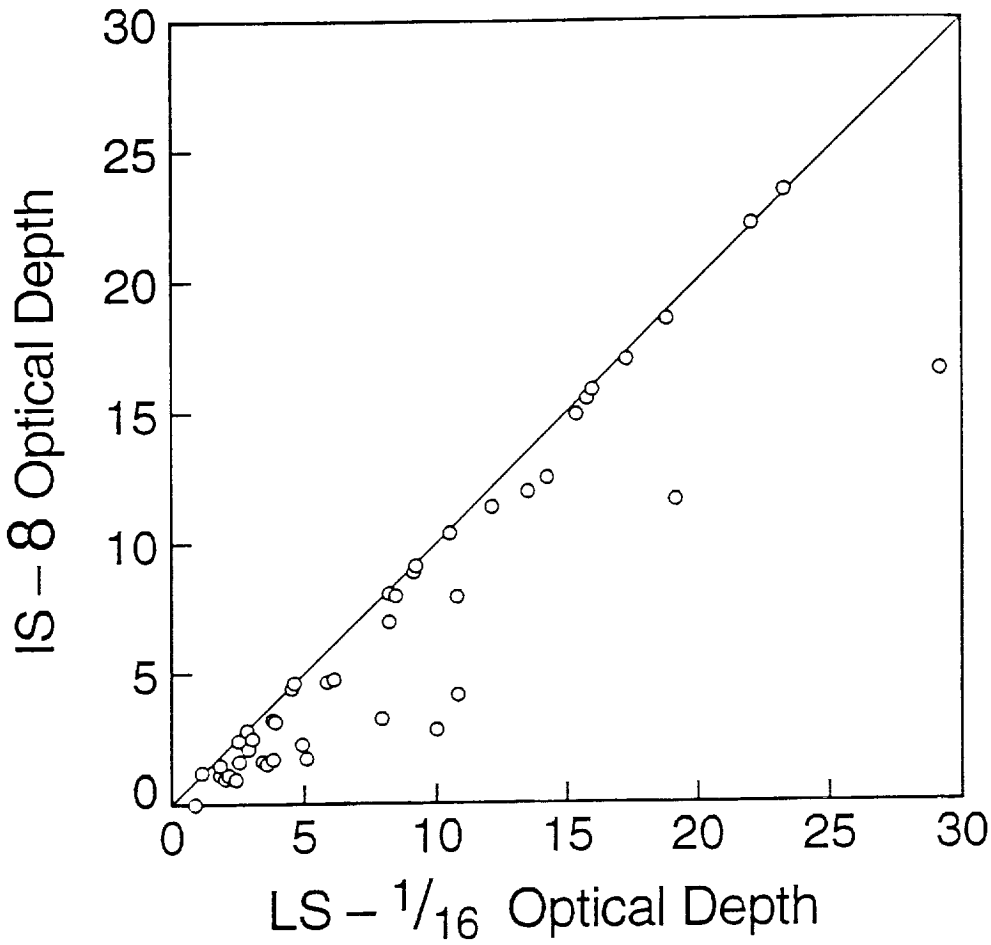
30
25
20
15
10
5
0
0
5
10
15
20
25
30
IS – 8 Optical Depth
LS – 1/16 Optical Depth

Figure 6

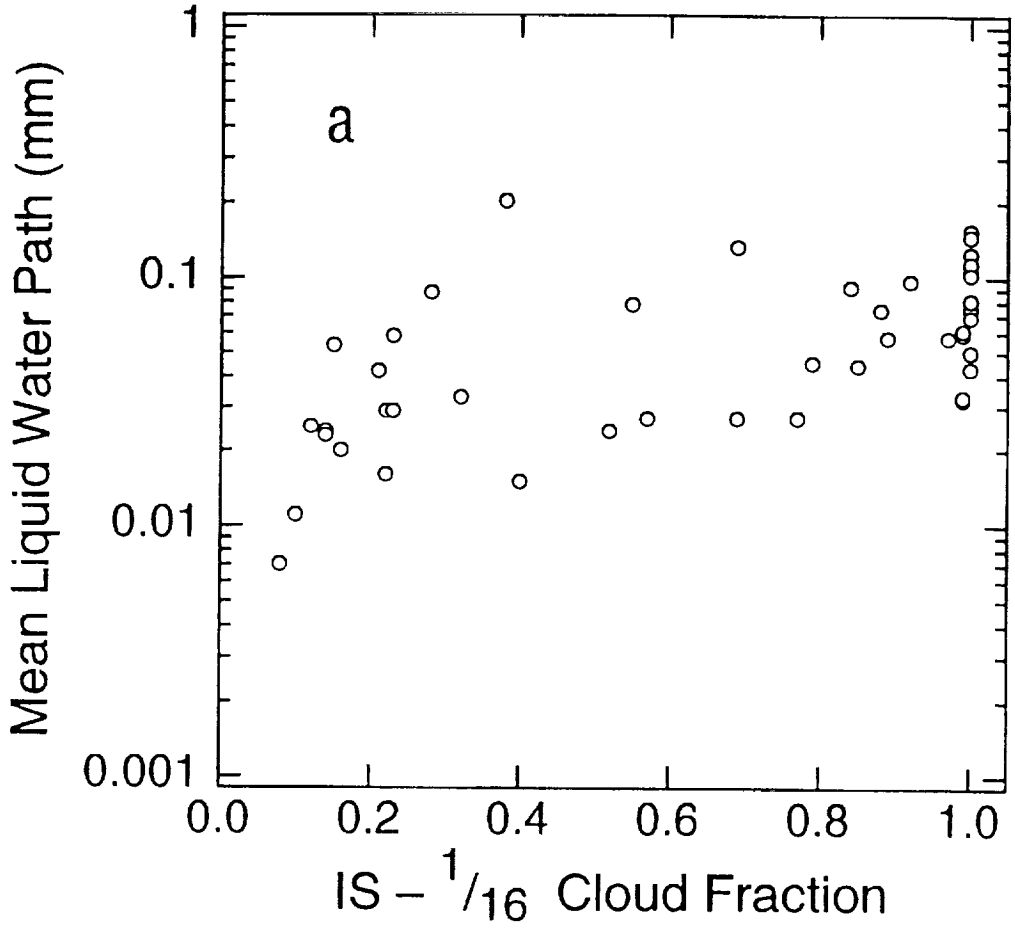
a
Mean Liquid Water Path (mm)
1
0.1
0.01
0.001
0.0
0.2
0.4
0.6
0.8
1.0
IS – 1/16 Cloud Fraction

Figure 7a

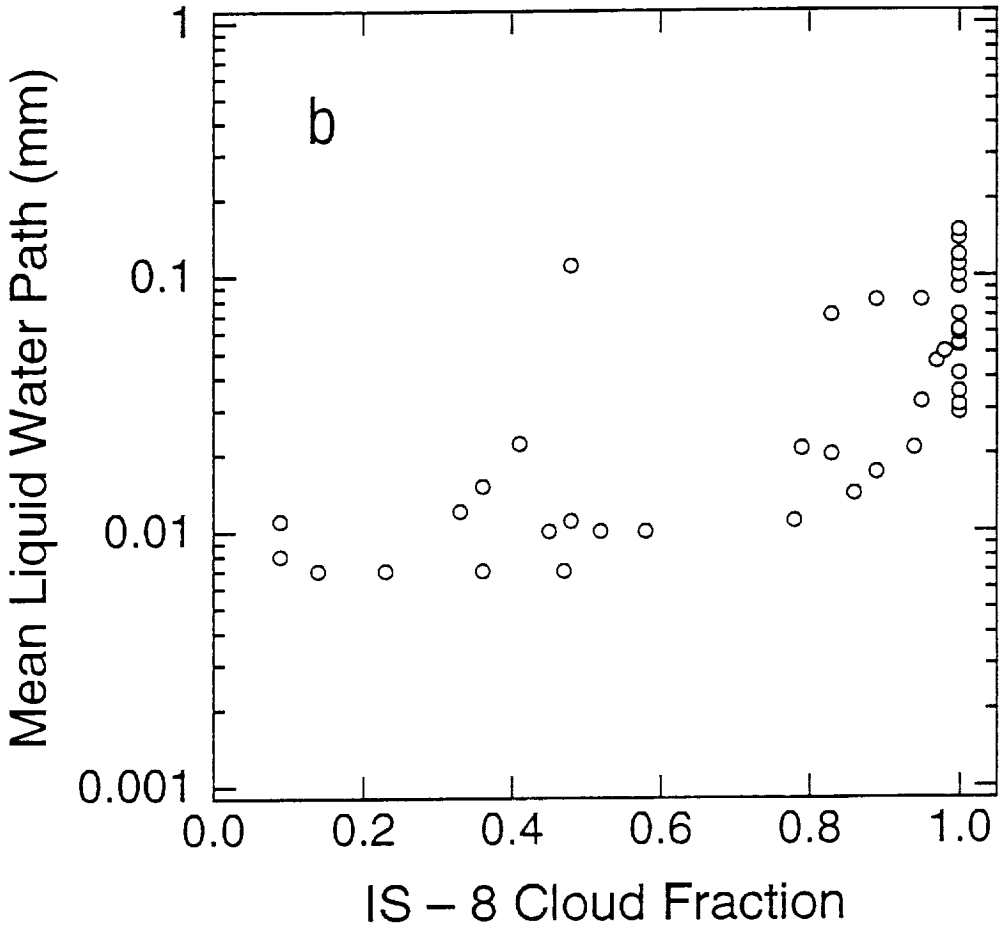
b
Mean Liquid Water Path (mm)
1
0.1
0.01
0.001
0.0
0.2
0.4
0.6
0.8
1.0
IS – 8 Cloud Fraction

Figure 7b

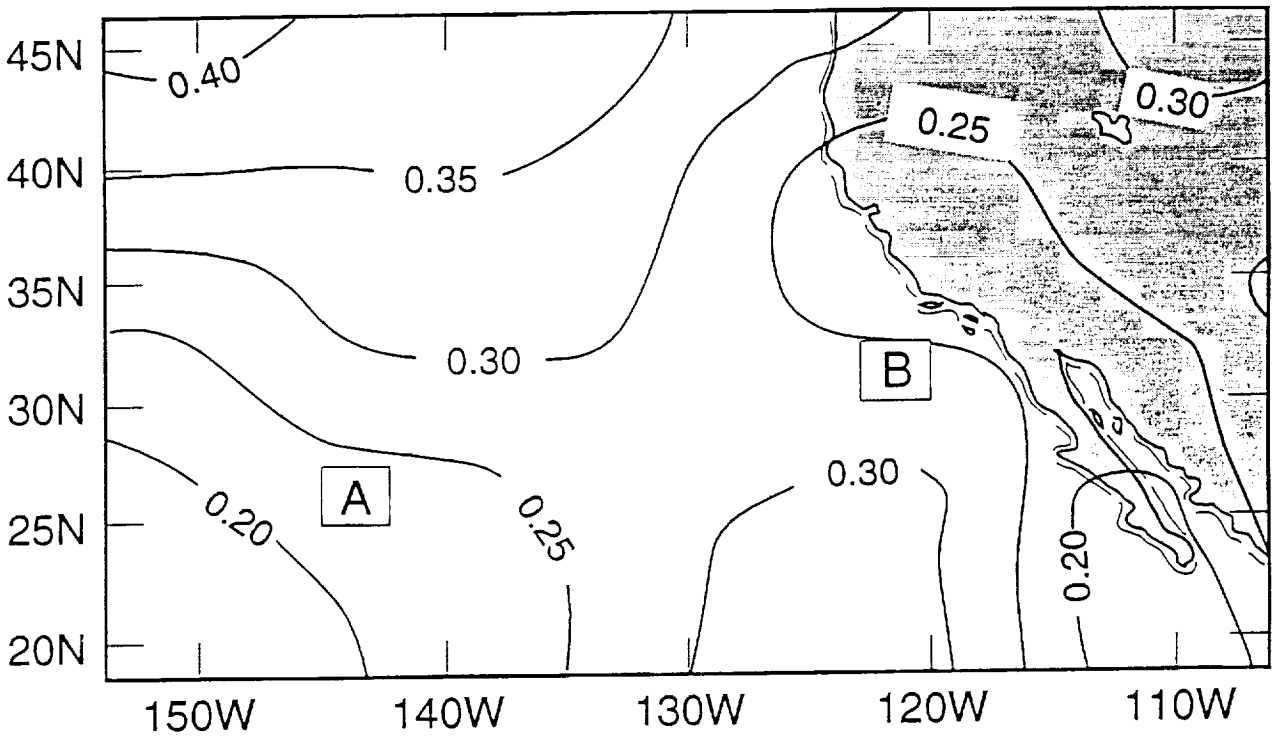
45N
40N
35N
30N
25N
20N
150W
140W
130W
120W
110W
0.40
0.35
0.30
0.20
0.25
0.30
0.25
0.30
0.20
A
B

Figure 8

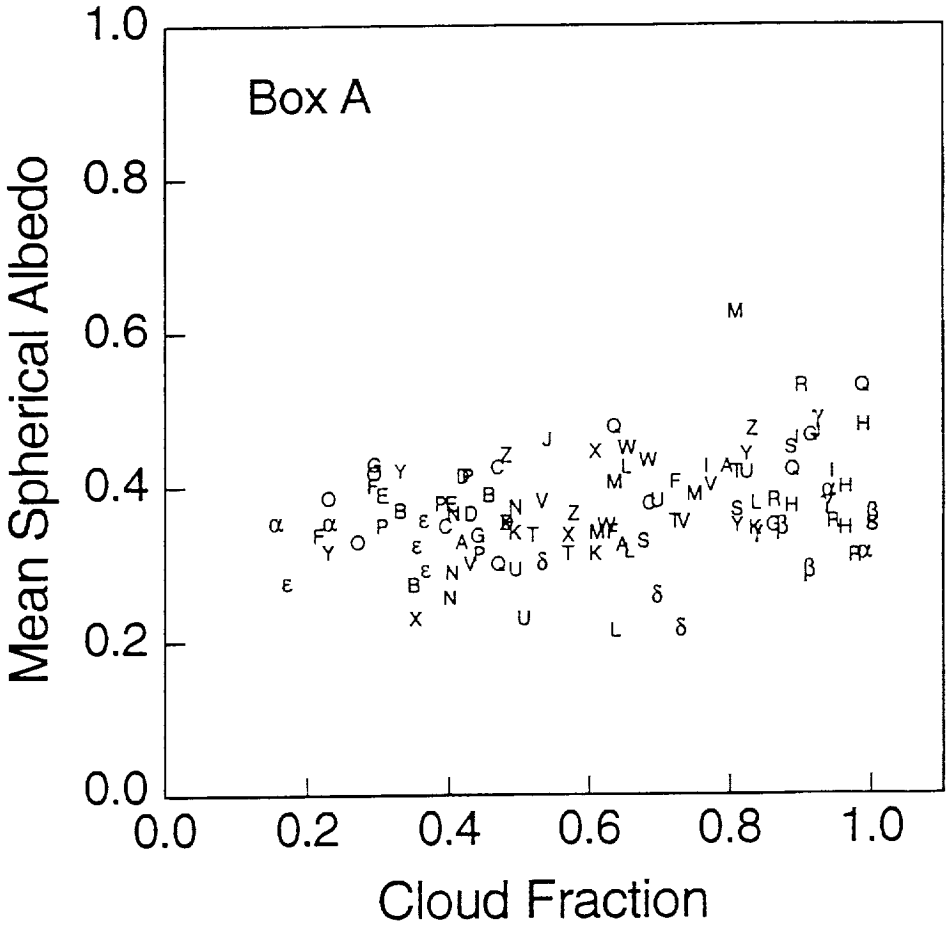

Figure 9

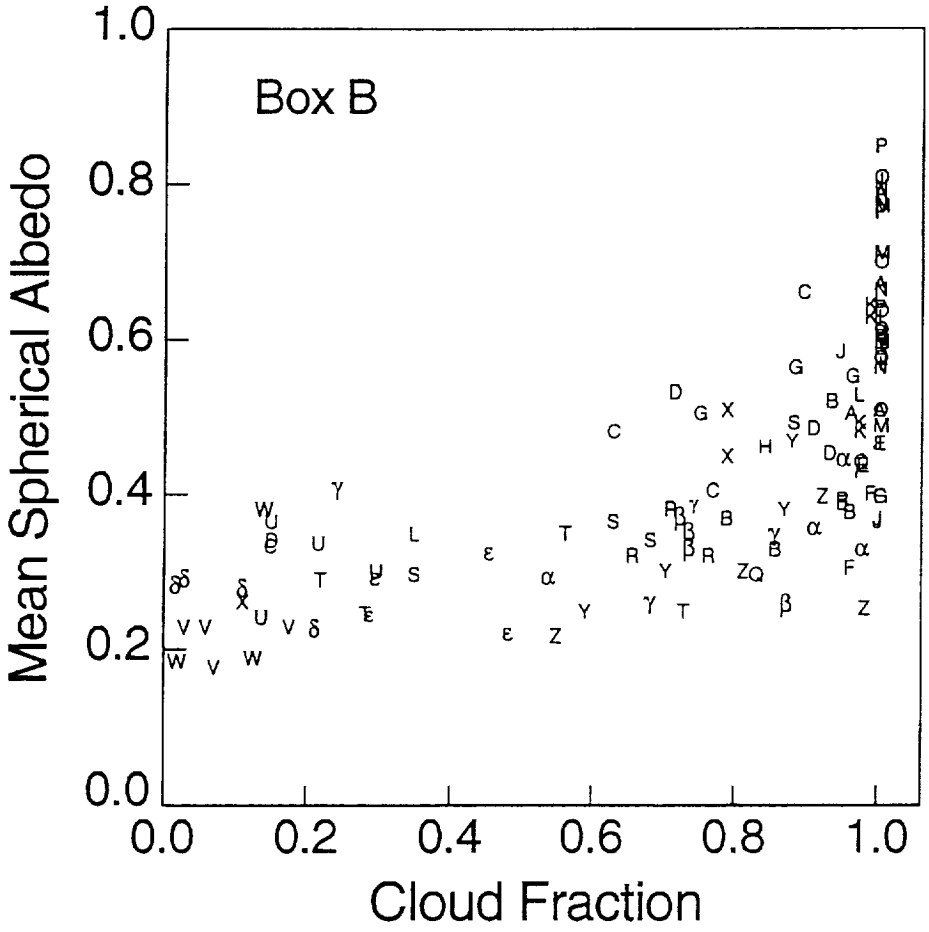

Figure 10